Recovering fluorescent spectra with an RGB digital camera and color filters using different matrix factorizations

Juan L. Nieves,* Eva M. Valero, Javier Hernández-Andrés, and Javier Romero

Departamento de Óptica, Facultad de Ciencias, Universidad de Granada, 18071 Granada, Spain

*Corresponding author: jnieves@ugr.es

The aim of a multispectral system is to recover a spectral function at each image pixel, but when a scene is digitally imaged under a light of unknown spectral power distribution (SPD), the image pixels give incomplete information about the spectral reflectances of objects in the scene. We have analyzed how accurately the spectra of artificial fluorescent light sources can be recovered with a digital CCD camera. The red-green-blue (RGB) sensor outputs are modified by the use of successive cutoff color filters. Four algorithms for simplifying the spectra datasets are used: nonnegative matrix factorization (NMF), independent component analysis (ICA), a direct pseudoinverse method, and principal component analysis (PCA). The algorithms are tested using both simulated data and data from a real RGB digital camera. The methods are compared in terms of the minimum rank of factorization and the number of sensors required to derive acceptable spectral and colorimetric SPD estimations; the PCA results are also given for the sake of comparison. The results show that all the algorithms surpass the PCA when a reduced number of sensors is used. The experimental results suggest a significant loss of quality when more than one color filter is used, which agrees with the previous results for reflectances. Nevertheless, an RGB digital camera with or without a prefilter is found to provide good spectral and colorimetric recovery of indoor fluorescent lighting and can be used for color correction without the need of a telespectroradiometer. © 2007 Optical Society of America

OCIS codes: 330.1710, 330.1730, 150.0150, 150.2950.

1. Introduction

Multispectral analysis and synthesis of the spectral power distribution (SPD) of illuminants and spectral reflectances has been explored extensively during recent years [1–9]. Spectral imaging combines the strength of conventional imaging with that of spectroscopy to accomplish tasks that each cannot perform separately. The product of a spectral imaging system is a stack of images of the same object or scene, each at a different spectral narrow band. The field is divided into techniques called multispectral, hyperspectral, and ultraspectral. While no formal definition exists, the difference is usually based on the number of bands. Multispectral deals with several images (from 6 to 31) at discrete and fairly narrow bands, which is what distinguishes multispectral in the visible from conventional red-green-blue (RGB) image capturing. Hyperspectral deals with imaging narrow spectral bands (up to 100) over a contiguous spectral range. Ultraspectral is typically reserved for interferometer-type imaging sensors with a very fine spectral resolution and deals with more than 100 bands. These sensors often have a low spatial resolution of several pixels only, a restriction imposed by the high data rate. These devices, when combined with computational image-processing algorithms, can produce the spectra of all the pixels in the scene. Therefore they are an alternative to the traditional spectroradiometers that have so far been used for this purpose, with their limited portability, low spatial resolution, and high cost. Different computational approaches have been introduced to improve both the spectral and colorimetric quality of spectral

recovery and to reduce the number of components needed to estimate the computed spectra [4–7,10–12]. When a scene is digitally imaged under an unknown light the image gives incomplete information about the spectral properties of the objects in the scene. Nevertheless spectral imaging is able to produce the spectral reflectance and/or spectral radiance of objects, which is of relevance in object and material recognition. In practice, imaging systems used to acquire scene reflectances have to be calibrated immediately after acquisition. This means that the light spectrum reflected from a neutral reference surface embedded in the scene should be recorded with a telespectroradiometer and the color signal at each pixel normalized against that derived from the white surface. Thus because of the time and money involved, spectral calibration may seriously limit the use of spectral imaging devices to derive simplified illuminant-independent images.

In a previous work we found that it was possible to recover daylight spectra with high spectral and colorimetric accuracy with a reduced number of spectral bands. We used an RGB camera with or without a prefilter (e.g., a CCD camera coupled or not with successive cutoff filters) and found with considerable accuracy a matrix that converted the camera outputs from a white paper to an estimated spectrum for the light [7]. The method, which we called direct pseudoinverse, was similar to the generalized pseudoinverse [13] and was based on an *a priori* analysis of the digital outputs generated by a training set of lights of known spectra. The results suggested that the direct pseudoinverse method surpasses methods based on eigenvector analysis with simple inversion and pseudoinverse transformation. The great advantage of this method when compared with many multiband imaging devices such as the liquid-crystal tunable filter (LCTF) is the simplification of the capture procedure using only three to nine spectral bands. The direct pseudoinverse algorithm was found to give good colorimetric performance with only six bands (e.g., the RGB camera without and with one cutoff filter) and confirmed the possibility of using a trichromatic RGB digital camera to recover daylight illuminants as well as spectral reflectances [8]. In addition it was unnecessary to use either the spectral sensitivities of the camera sensors or eigenvector analysis. The training set of illuminants was clearly dominated by daylight spectra, and thus narrow and prominent emission peaks at certain wavelengths did not influence the analysis. We found that it was difficult to obtain a low-dimension basis to accommodate the diversity of a complete set of commercial fluorescent sources [10]. Using a global basis, which included daylight and blackbody spectra and the standard illuminants of the CIE, the SPD recoveries of commercial fluorescents, though acceptable, especially for colorimetric purposes, could not be considered completely satisfactory at least for spectral purposes. The direct pseudoinverse approach does not use eigenvectors and may prove to be a good alternative to spectral devices that need to estimate indoor illumination.

Different approaches have been proposed for classifying and characterizing fluorescent scene illumination based on a classification procedure with a reduced set of tabulated fluorescents instead of recovering their spectral profiles. Tominaga *et al*. [14–17] used an LCTF coupled with a monochrome CCD camera and approached the problem with a proposal including two different methods. On the one hand, they used an illuminant classification algorithm based on a gamut-based correlation between image colors and a reference illuminant gamut of colors, and on the other, a peak-detection technique to analyze the second derivative spectrum throughout the multiple images captured by their device. Although the latter procedure used neither a linear model nor the color temperature of the illuminants, the classification results were constrained into only three groups of fluorescent lights.

Multispectral imaging techniques have been applied to the recovery of spectral reflectances, SPDs of illuminants and spectral radiances either by exploiting the smoothness of the reflectance spectra, using low-dimensional linear models, or by determining empirical relationships between spectra and digital counts [18,19]. Apart from finite-dimensional models of spectra based on principal component analysis (PCA), methods such as independent component analysis (ICA) and nonnegative matrix factorization (NMF) have been developed as alternative mathematical approaches to describing spectral functions. ICA seeks to represent multivariate signal data in a linear nonorthogonal system by maximizing the mutual statistical independence of the source signals. The basis functions derived from ICA are not orthogonal and are defined by second- and higher-order statistics of the data and are as statistically independent as the data allow; this is an important difference when compared with the orthogonal bases obtained from PCA. NMF algorithms also seek a linear representation similar to that derived from ICA, but they impose an additional nonnegativity constraint in that only additive linear combinations of basis functions are allowed. These mathematical techniques have proved to be of particular interest in the design of physically realizable sensors for recovering spectral functions [20]; thus the algorithms are used to derive appropriate bases for identifying the pseudoinverse of the basis vectors with the optical sensors to be used by a spectral device. The methods have also been a subject of study by comparing their performance for spectral recovery of reflectances and color signals, with ICA giving a compression index comparable to JPEG but with more complex computations [21].

The aim of our present work was to analyze how well the spectra of artificial fluorescent light sources could be recovered with a digital CCD camera. The RGB sensor outputs were modified by the use of successive cutoff color filters; we used one or two broadband color filters to increase the number of spectral bands of the camera. We evaluated the spectral and colorimetric recovery of incandescent and fluorescent illuminants using nonnegative matrix factorization, independent component analysis, and a direct pseudoinverse ap-

proach. Computational and experimental results are shown with or without a prefilter. None of the recovery algorithms used here needed information about the spectral sensitivities of the camera sensors or eigenvectors to estimate the spectral power distributions of illuminants. The different mathematical algorithms have been compared in terms of the number of sensors and dimensionality reduction (rank of factorization) with particular interest in how the algorithms recovered the spiky spectral profiles that characterize the SPDs of fluorescents. Because of the difficulties involved in recovering these spiky SPDs with most linear algorithms we also analyzed a classification of artificial illuminants with reduced computational cost with the idea of reaching a compromise between perfect spectral recovery (e.g., illuminant identification for color constancy) and the minimum possible number of spectral descriptors to allow an acceptable spectral and colorimetric description of indoor illumination.

2. Illuminant-Recovery Methods

When a CCD digital color camera is pointed at a surface with spectral reflectance function $r^x(\lambda)$, the response of the kth sensor for pixel x can be modeled linearly by

$$\rho_k{}^x = \sum_{\lambda=400}^{700} E^x(\lambda) r^x(\lambda) Q_k(\lambda) \Delta\lambda, \tag{1}$$

where $Q_k(\lambda)$ is the spectral sensitivity of the kth sensor, and $E^x(\lambda)$ is the SPD of the illuminant impinging on the surface, both functions sampled at 5 nm intervals in the visible range of 400–700 nm. Thus Eq. (1) can be rewritten in matrix notation as

$$\rho = \mathbf{CE}, \tag{2}$$

where ρ is a $k \times N$ matrix the columns of which contain the sensor responses for each of the N image pixels, and $\mathbf{C}$ is a $k \times n$ matrix ($n = 61$ wavelengths) the rows of which contain the wavelength-by-wavelength multiplication of the reference white surface reflectance and sensor sensitivities. As we showed in a previous study [7] a linear system of k equations with n unknowns should be resolved from Eq. (2) to determine the SPD $\mathbf{E}$ if the spectral reflectance r of a reference surface embedded in a scene and its corresponding digital counts ρ are known. To solve this underestimation problem, the number, k, of the camera sensors can be increased by using successive cutoff filters in front of the camera lens as each cutoff filter generates three new sensitivity curves. Thus we are increasing the number of degrees of freedom and have more equations to solve for more possible unknowns [7,19,22,23].

We first simulated digital counts using the spectral sensitivities of a Retiga 1300 digital CCD color camera (QImaging Corp., Canada) with 12 bits intensity resolution per channel. We assume that the camera is pointing at chip number 19 from the ColorChecker, X-Rite Inc. and GretagMacbeth AG, USA, which has a known spectral reflectance, and modeled the CCD response according to Eq. (2). Matrix $\mathbf{C}$ in Eq. (2) is
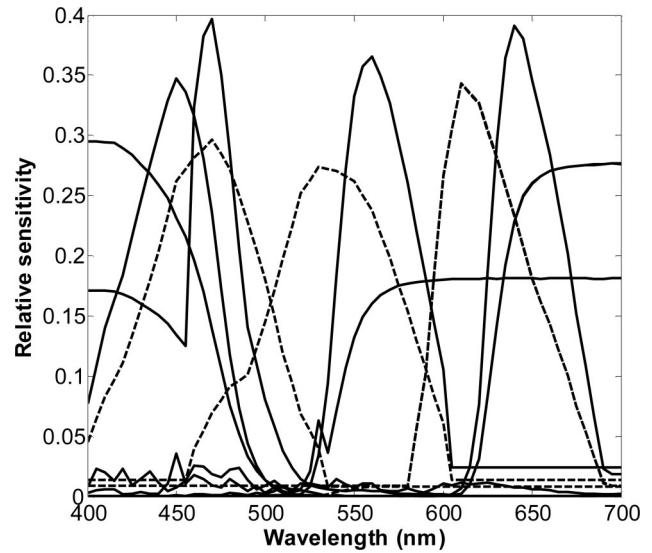

Fig. 1. Spectral sensitivities of the 3-, 6-, 9-, and 12-band spectral camera. Dashed and solid curves represent the unmodified and modified bands of the RGB digital camera sensors, respectively. The successive cutoff filters were the OG550, RG630, and BG12 colored-glass filters from OWIS GmbH.

based on a set of camera sensitivities but is used to generate only a set of noise-free fictitious data. The algorithms being tested then proceed without using the camera's sensitivity data. The RGB camera outputs are modified to use a 3-, 6-, 9-, or 12-band spectral camera (Fig. 1); in this way the number of sensors was $k = 3, 6, 9,$ or 12. The colored filters were colored glass filters OG550, RG630, and BG12 from OWIS GmbH, Staufen, Germany.

Following the usual procedure we used a set of spectra for training and a different set for testing the performance of the algorithms. The training set was composed of 82 SPDs of fluorescent-type illuminants, and the test set comprised a set of 20 commercial fluorescent and incandescent lights that were not included in the training set [24]. The training set included the common three groups into which the SPDs of fluorescents are usually categorized according to their spectral profile (the common fluorescents F1 to F6, the high-color-rendering fluorescents F7 to F9, and the triple-band fluorescents F10 to F12) [25]. Figure 2 shows the color distributions in the CIELab a*b* space when the white surface was illuminated by each illuminant from the training and test sets. Equation (2) was used to derive the digital counts under different illuminant conditions, and these fictitious data acted to simulate the camera in Section 3. Different mathematical approaches were used to resolve Eq. (2) for the SPDs of the illuminants.

A. Nonnegative Matrix Factorization Algorithms

Given a nonnegative data matrix, $\mathbf{E}$ (an $n \times m$ matrix), nonnegative matrix factorization finds an approximate factorization into two nonnegative matrix factors, $\mathbf{W}$ (an $n \times u$ matrix of basis vectors) and $\mathbf{H}$ (a $u \times m$ matrix of u coefficient vectors), where the
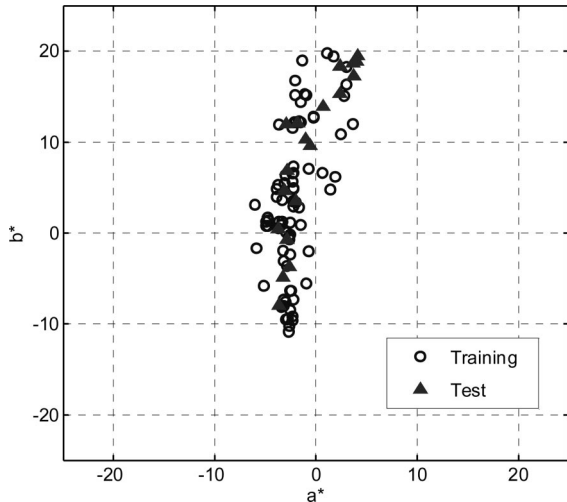
Fig. 2. The CIELab a*b* color distributions obtained for chip 19 of the MacBeth ColorChecker under each of the training and test illuminants.

so-called rank of factorization, u, is smaller than either n or m and allows us to introduce the general concept of dimensionality reduction and its relationship to matrix factorization [26,27]. In this work the data matrix is a set of unknown illuminant spectra, $\mathbf{E}$ (an $n \times m$ matrix of $m = 20$ illuminant spectra sampled at $n = 61$ wavelengths in the visible range of 400–700 nm), which will be derived using a relationship involving the coefficient vector within each column of $\mathbf{H}$ (an $u \times m$ matrix) as

$$\mathbf{E} = \mathbf{W}\mathbf{H}. \tag{3}$$

Since the intention of spectral recovery is to estimate the illuminant spectra from the responses of a CCD color camera, we first computed a set of sensor outputs, $\boldsymbol{\rho}_o$ (a $k \times t$ matrix of $t = 82$ training spectra captured by k sensors) and coefficient matrix, $\mathbf{H}_o$ (a $u \times t$ matrix), from a training set of illuminants. Thus, given a data matrix of unknown illuminant spectra, $\mathbf{E}$, the sensor outputs of which are $\boldsymbol{\rho}$ (a $k \times m$ matrix), the corresponding coefficient matrix, $\mathbf{H}$, is computed from the training set as

$$\mathbf{H} = \left[\mathbf{H}_o\left(\boldsymbol{\rho}_o{}^T\boldsymbol{\rho}_o\right)^{-1}\boldsymbol{\rho}_o{}^T\right]\boldsymbol{\rho} = \left(\mathbf{H}_o\boldsymbol{\rho}_o{}^+\right)\boldsymbol{\rho}, \tag{4}$$

where $\boldsymbol{\rho}_o{}^+$ is the pseudoinverse matrix of $\boldsymbol{\rho}_o$. Equation (3) is then applied to recover the estimated spectra. To reduce the computational cost of spectral estimation the rank of factorization, u, can be adjusted according to the input data matrix. We have resorted to two NMF algorithms, which use two different error functions for the optimum choice of $\mathbf{W}$ and $\mathbf{H}$, these being the Euclidean and the divergence updates by Lee and Seung [28].

B. Independent Component Analysis Algorithm

Independent component analysis (ICA) is a statistical, computational technique for developing the hid-

den factors that underlie sets of random variables and measurements. The ICA algorithm approximates data using a similar decomposition to that in Eq. (3) and finds basis vectors that are uncorrelated and also independent but not necessarily orthogonal. The data variables are assumed to be linear mixtures of some unknown latent variables and the mixing system is also unknown. The latent variables are assumed to be non-Gaussian and mutually independent, and are known as the independent source or factor components of the observed data [27,29]. ICA assumes that the data set $\mathbf{E}$ can be represented as a linear combination of a set of independent source components, h_i. Thus $\mathbf{E} = \mathbf{W}\mathbf{H} = \sum_i w_i h_i$, where $\mathbf{W}$ is a scalar square matrix and the rows of $\mathbf{W}$ (components w_i) are the basis functions. Note that the data set $\mathbf{E}$ has the same meaning as it does in the NMF calculations. Thus, assuming a set of unknown illuminant spectra, $\mathbf{E}$ (an $n \times m$ matrix of $m = 20$ illuminant spectra), we can follow the same steps as in the derivation of Eqs. (3) and (4) to recover the estimated spectra. We used here the fast-ICA algorithm by Hyvarinen [29], which is a computationally highly efficient and faster method for performing the estimation of ICA.

C. Direct Pseudoinverse Method

This method is also based on a pseudoinverse transformation between the estimated illuminant spectra, $\mathbf{E}$, (an $n \times m$ matrix, with $m = 20$) and sensor responses, $\boldsymbol{\rho}$ (a $k \times m$ matrix) expressed by

$$\mathbf{E} = \mathbf{F}\boldsymbol{\rho}. \tag{5}$$

In this expression matrix $\mathbf{F}$ (an $n \times k$ matrix) is derived following a pseudoinverse method by

$$\mathbf{F} = \mathbf{E}_o\left[\left(\boldsymbol{\rho}_o{}^T\boldsymbol{\rho}_o\right)^{-1}\boldsymbol{\rho}_o{}^T\right] = \mathbf{E}_o\boldsymbol{\rho}_o{}^+, \tag{6}$$

where $\mathbf{E}_o$ (an $n \times t$ matrix, with $t = 82$) and $\boldsymbol{\rho}_o$ (a $k \times t$ matrix) are the SPDs, and their corresponding sensor outputs for the training set of illuminants and $\boldsymbol{\rho}_o{}^+$ are the pseudoinverse matrices of $\boldsymbol{\rho}_o$ [7]. Equation (5) is equivalent to an analysis in which an orthonormal basis such as the orthonormal basis of the sensor output vectors is found.

D. Principal Component Analysis

Principal component analysis (PCA) is the most usual approach for reducing multidimensional datasets to lower dimensions. It is based on the fact that it is possible to find square-integrable functions $V_i(\lambda)(i = 1, 2, \ldots, M)$ and a single set of real numbers, ε_i, such that $E(\lambda) = \sum_{i=1}^{M} \varepsilon_i V_i(\lambda)$ where coefficients ε_i are obtained by orthogonal projection over the basis functions [22]. Most of the SPDs of natural illuminants can be described by small-dimensional linear models and earlier studies have shown that 3 to 7 eigenvectors, which can be obtained by PCA, suffice for adequate reconstructions of the illuminants [9–12,23]. Using Eq. (2) and this linear representation, a two-step $M \times k$ transformation is derived by fitting the k digital signals and the M eigenvector coefficients, ε_i.

A relationship between the sensor camera and the digital counts can be established by the usual pseudo-inverse calculations [7] as

$$\mathbf{G} = \varepsilon \boldsymbol{\rho}^T [\boldsymbol{\rho}\boldsymbol{\rho}^T]^{-1}, \qquad (7)$$

and the estimated SPDs of the illuminants can be obtained from the matrix product

$$\mathbf{E}_e = \mathbf{V}(\mathbf{G}\boldsymbol{\rho}). \qquad (8)$$

The method requires a careful choice of k sensors since their number determines the dimension of the base derived from PCA and influences the spectral and colorimetric quality of the SPD estimation [4,5].

E. Metrics for Quality Evaluation and Classification

To quantify the quality of the reconstructions we used the following metrics: the goodness-of-fit-coefficient (GFC) and the CIELab color difference, ΔE_{ab}^* [30,31]. The GFC is based on Schwartz's inequality and is defined as the cosine of the angle between the original signal $f(\lambda)$ and the recovered signal $f_r(\lambda)$, thus

$$\mathrm{GFC} = \frac{\left| \sum_j f(\lambda_j) f_r(\lambda_j) \right|}{\left[\left| \sum_j [f(\lambda_j)]^2 \right| \left| \sum_j [f_r(\lambda_j)]^2 \right| \right]^{1/2}}. \qquad (9)$$

This measurement of spectral similarity has the advantage of not being affected by scaled factors. Colorimetrically accurate illuminant estimations require GFC > 0.995; GFC > 0.999 indicates quite good spectral fit, and GFC > 0.9999 an almost-exact fit [12]. The CIELab color-difference formula was used to evaluate colorimetric quality and was calculated with reference to the color signal of a white patch in the scene for illuminant estimation; a D65 illuminant was assumed for the evaluation of color differences. Differences of less than 3 CIELab units between the original and the estimated spectra were considered to be acceptable [30–33].

3. Computational Results

We made an experiment to evaluate the performance of the above methods first using simulated digital counts. Subsequently, we used a real RGB digital camera, the same as that described to compute the digital counts. The experimental setup is dealt with in Section 4.

A. Comparison Between Methods

To analyze the differences between the various recovery algorithms we first used the same SPDs for both the training phase, according to Eqs. (4) and (6), and the test phase to study the spectral recovery performance. Figure 3 illustrates the average colorimetric (ΔE_{ab}^*) performances when the algorithms are used
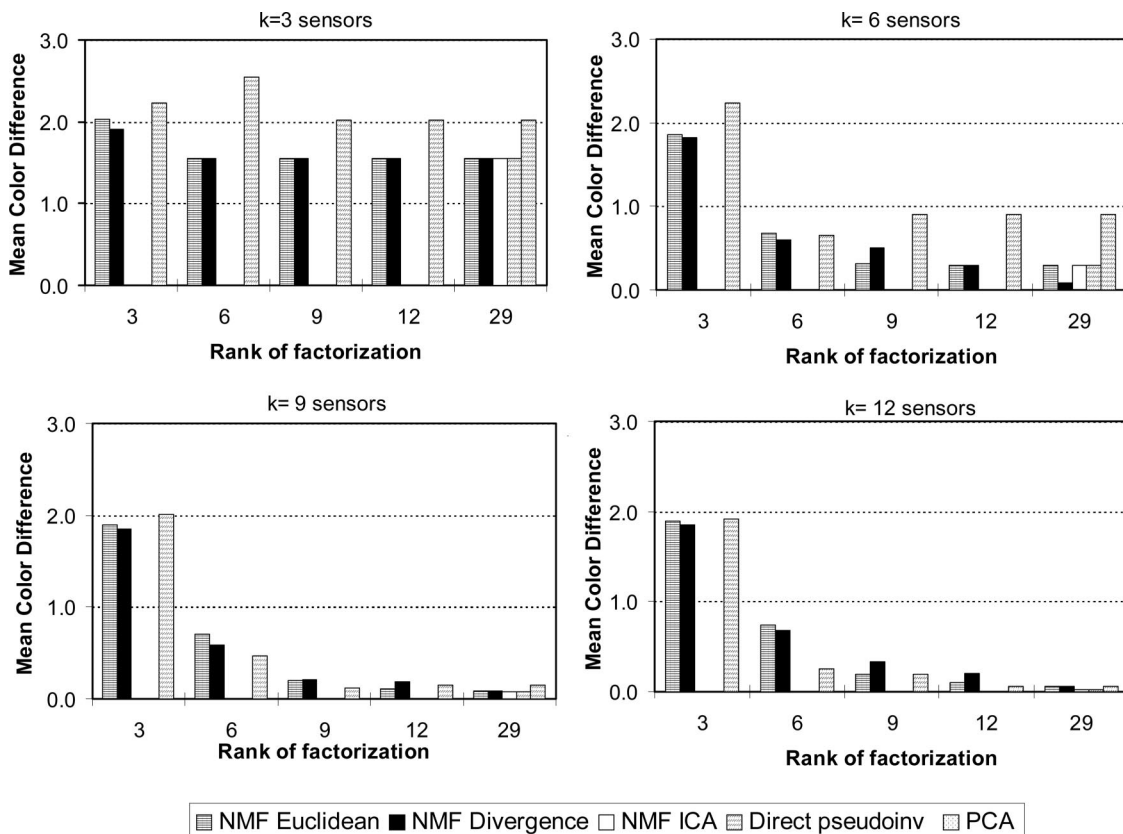

Fig. 3.   CIELab color differences derived from the algorithms tested using different numbers of sensors and factorization rank. The results are mean values for the training set of fluorescent illuminants.

| Measure | Algorithm | Number of Sensors | | | | | | | |
| | | $k = 3$ | | $k = 6$ | | $k = 9$ | | $k = 12$ | |
		Mean	SD	Mean	SD	Mean	SD	Mean	SD
GFC	NMF Euclidean	0.98004	0.04226	0.98004	0.04226	0.98004	0.04226	0.99972	0.00054
	NMF divergence	0.98004	0.04226	0.98004	0.04226	0.98004	0.04226	0.99972	0.00059
	ICA	0.98005	0.04225	0.99704	0.00701	0.99920	0.00220	0.99973	0.00053
	Direct pseudoinv	0.98005	0.04225	0.99704	0.00701	0.99920	0.00220	0.99973	0.00053
	PCA	0.96405	0.04509	0.97663	0.04030	0.99316	0.01640	0.99803	0.00350
ΔE*ab	NMF Euclidean	1.5467	1.3898	0.2912	0.2834	0.0909	0.1215	0.0567	0.0631
	NMF divergence	1.5484	1.3962	0.0860	0.1194	0.0860	0.1194	0.0615	0.0616
	ICA	1.5484	1.3958	0.2920	0.2860	0.0819	0.1215	0.0228	0.0424
	Direct pseudoinv	1.5484	1.3958	0.2920	0.2860	0.0819	0.1215	0.0228	0.0424
	PCA	2.0200	1.3700	0.9005	1.2500	0.1522	0.2223	0.0620	0.0853

[a]Only the maximum rank of factorization ($u = 29$ in the case of NMF algorithms) is shown for each number of filters.

with different ranks of factorization for the training set of illuminants. The rank of factorization $u = 29$ was chosen according to the convergence rate derived from the original ICA algorithm [28]. It should be noted that where no bars appear in the figures it means that the algorithm does not converge appropriately (e.g., ICA for $u < 29$ coefficients) or that it makes no sense (e.g., direct pseudoinverse algorithm, as it does not use coefficients).

The recovery colorimetric quality clearly improves concomitantly with an increase in both the number of camera filters and the rank of factorization. The results show that even with only three sensors the color differences are approximately or less than 2 CIELab units (which indicates a good colorimetric estimation) for all methods. PCA always provides the worst results, but this is an expected result because of the spiky spectral profiles of the SPDs, which correspond to the SPDs of the fluorescent lights that we used here. By introducing more color filters the recovery quality is significantly better (less than 0.2 CIELab units for two color filters and the maximum rank of factorization). Table 1 shows the mean GFC and

ΔE*ab values calculated across all the training illuminant spectra; only results from the maximum rank of factorization are shown for color filter combinations. The results show very good spectral recoveries for 9 and 12 sensors with GFC values above 0.999 for the NMF, ICA, and direct pseudoinverse algorithms. In addition, our results suggest that the ICA and direct pseudoinverse approaches lead to very similar results and surpass NMFs for 6 and 9 sensors. In a previous work we found that daylight spectra could be recovered with a reduced number of sensors based on an *a priori* analysis of a set of RGB signals from a white surface captured by a digital CCD camera [7]. The results shown here from the ICA and the direct pseudoinverse methods confirm the CCD's potential as an illuminant-estimation device even for a reduced training set of illuminants and the spiky profiles of some of these SPDs.

The advantage of the NMF algorithm is that we can adjust the size of the coefficient matrix, **H**, to minimize the computational cost of SPD recovery. The effects of rank of factorization and number of filters were tested by a repeated-measured analysis

| Measure | Algorithm | Number of Sensors | | | | | | | |
| | | $k = 3$ | | $k = 6$ | | $k = 9$ | | $k = 12$ | |
		Mean	SD	Mean	SD	Mean	SD	Mean	SD
GFC	NMF Euclidean	0.95062	0.06239	0.97873	0.02209	0.97961	0.02272	0.98474	0.02428
	NMF divergence	0.95065	0.06240	0.97949	0.02280	0.97949	0.02280	0.98431	0.02501
	ICA	0.95062	0.06240	0.97870	0.02207	0.97981	0.02238	0.98472	0.02492
	Direct pseudoinv	0.95065	0.06240	0.97873	0.02205	0.97984	0.02236	0.98480	0.02489
	PCA	0.89926	0.07683	0.94410	0.04599	0.98543	0.01167	0.93557	0.10765
ΔE*ab	NMF Euclidean	1.9421	1.7096	0.7395	0.7485	0.4043	0.4300	0.2886	0.3435
	NMF divergence	1.9479	1.7170	0.3926	0.3946	0.3926	0.3946	0.3297	0.3180
	ICA	1.9464	1.7161	0.7438	0.7472	0.3625	0.3400	0.2142	0.3082
	Direct pseudoinv	1.9467	1.7169	0.7451	0.7473	0.3621	0.3406	0.2118	0.3085
	PCA	3.0078	1.5298	1.8320	1.3003	0.4600	0.2593	0.6372	0.9146

[a]Only the maximum rank of factorization ($u = 29$ in the case of NMF algorithms) is shown for each number of filters.

of variance (ANOVA) of three factors: the *algorithm* (three levels: NMF Euclidean, NMF Divergence, and PCA), the *number of sensors* (four levels: $k = 3, 6, 9,$ or 12) and the *rank of factorization* (five levels: $u = 3, 6, 9, 12,$ or 29). Thus we first analyzed the statistical differences between the NMF and PCA algorithms using a $3 \times 4 \times 5$ multivariate analysis of variance (MANOVA) because ICA and direct pseudoinverse methods do not allow different ranks of factorization. We found significant differences for GFC ($p \ll 0.05$) depending upon the algorithm, number of sensors, and the ranks of factorization to be used. Our results suggest no interaction between the factors *algorithm* and *rank u*, although it is close to significant ($p = 0.059$). Post hoc comparisons do not suggest significant differences between NMF Euclidean and NMF Divergence ($p = 1.00$), although the difference between them and PCA is significant ($p \ll 0.05$), as shown in Table 1. For the factor *sensor* we found significant differences in the GFC values as a function of the number of color filters used, although values are close to significance level ($p = 0.023$) for two- and three-color filters ($k = 9$ and $k = 12$, respectively) suggesting asymptotic values for GFC when more than two color filters are used. We did not find the triple interaction among factors to be significant ($p = 0.729$).

As far as the colorimetric differences are concerned, our results show significant differences for the three factors ($p \ll 0.05$), with the double interaction *algorithm $\times$ rank* and *sensor $\times$ rank* being significant but not the triple interaction ($p = 0.628$). Once more, post hoc analysis suggests significant differences between the NMF and PCA algorithms ($p \ll 0.05$), but no differences are found between NMF Euclidean and NMF Divergence. The number of filters used is also significant for colorimetric quality, suggesting an asymptotic value for color differences (in this case values are close to significance with $p = 0.059$). On the other hand, the factor *rank* is significant for colorimetric quality, with the largest differences found for $u = 3$, whatever the algorithm and number of sensors used.

We then included ICA and direct pseudoinverse into the statistical analysis by fixing $u = 29$ for NMFs and PCA. A 3×4 MANOVA shows that the factors *algorithm* and *sensor* and their corresponding interactions are significant ($p \ll 0.05$) for spectral and colorimetric quality. Post hoc analysis shows that PCA obtained the worst results, both for spectral quality (average GFC value of 0.9800 versus 0.9940 for the other algorithms) and colorimetric quality (average ΔE^*ab of 0.78 versus 0.48 for the others). The difference between the use of two or three filters is close to significant ($p = 0.03$), confirming a maximum quality for more than two color filters. The statistical results show that the larger differences correspond to the use of a naive RGB camera (GFC value of 0.997 and ΔE^*ab of 1.642 on average for all factors). Thus we can conclude that introducing more than two colored filters is unlikely to produce significant improvement in spectral and colorimetric quality, with PCA

deriving the worst results. In addition, a reduction of dimensionality to $u = 3$ clearly affects colorimetric quality whatever the algorithm and number of colored filters used.

B. Spectral and Colorimetric Qualities for Test Spectra

We use here the test set of illuminants, which are not included in the training data set, to analyze the performance of the recovery algorithms. Table 2 shows the mean (and sample standard deviation) of GFC and ΔE^*ab values calculated across all test spectra for each number of filters and the maximum rank of factorization. First, the results confirm that both recovery quality and performance increase concomitantly with the number of sensors, as expected from previous results. The values are above 0.984 for GFC and around 0.2 ΔE^*ab for color differences when the maximum number of sensors are used, but not for PCA. We find that the spectral-recovery quality derived from PCA is poor, even for $k = 12$ sensors (GFC approximately 0.935), although the colorimetric qual-
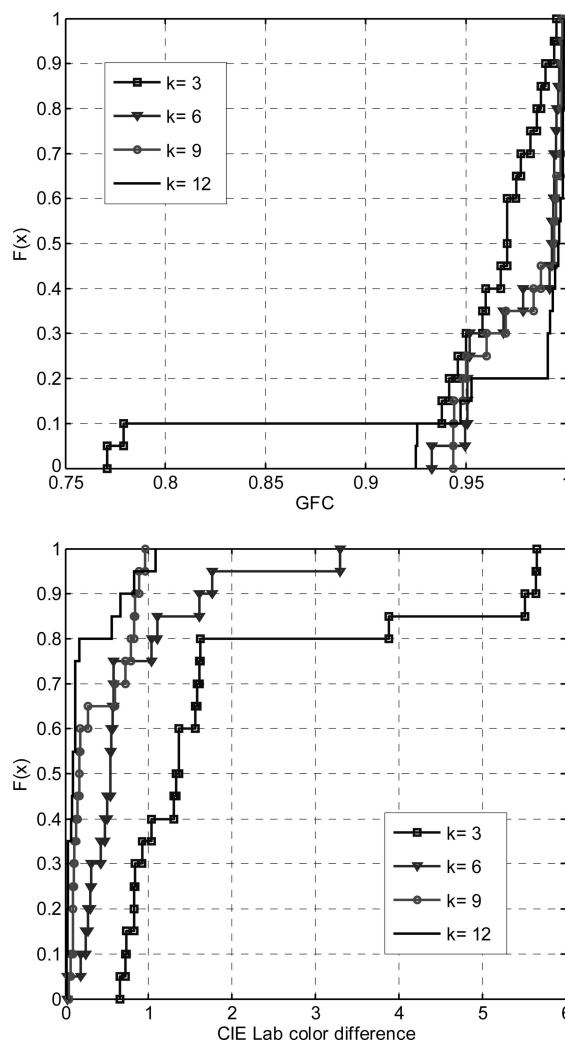

Fig. 4. Cumulative distribution function for the GFC (upper plot) and color difference (lower plot) data derived from the direct pseudoinverse method. The results are for the test set of fluorescent illuminants and different numbers of sensors.

ity is acceptable, with color differences of around 0.6 ΔE*ab for the best result.

Second, metric selection is crucial for the spiky spectral profile of fluorescents. Figure 4 shows the cumulative distribution function for the spectral and colorimetric performance derived from the direct pseudoinverse method. The figure shows the proportion of spectral recoveries that takes on values less than or equal to some GFC and ΔE*ab values. What is clear is that the variety of fluorescents comprising the test illuminant set now leads to lower average GFC values. Nevertheless, the colorimetric quality is acceptable for three sensors (7 of 20 test fluorescents lead to ΔE*ab > 2) and very good when the camera is combined with color filters. Figure 5 shows examples of spectral recovery for fluorescent illuminants with different spectral profiles and using different numbers of sensors. The examples on the top row are for spectrally and colorimetrically accurate illuminant estimations with GFC > 0.995 and ΔE*ab ≪ 1 and those on the bottom row are from colorimetrically accurate estimations with low color differences but lower spectral quality according to GFC values. These examples clearly reveal the differences between spectral and colorimetric metrics when prominent spectral emission peaks appear in the SPD of fluorescents. This is particularly evident for those illuminants that show a relatively smooth spectral profile, for which the recoveries are far from being spectrally accurate (see Fig. 5). Nevertheless, color differences are below 2 CIELab units between the original and the estimated spectra and thus can be considered acceptable [18,30,31]. We have tested the differences between spectral and colorimetric qualities using a 5 × 4 MANOVA, which includes the effects of the *algorithm* and the *number of sensors*. For both GFC and color differences we found no significant differences between the algorithms ($p \gg 0.05$) and the statistical influence on the number of color filters used ($p = 0.002$). We did find, however, significant interaction between the algorithm and the number of sensors for the measurement ΔE*ab ($p \ll 0.05$) while there was no interaction for the factor GFC ($p = 0.544$). Thus the statistical analysis suggests that spectral estimation is a multidimensional problem and a combination of different
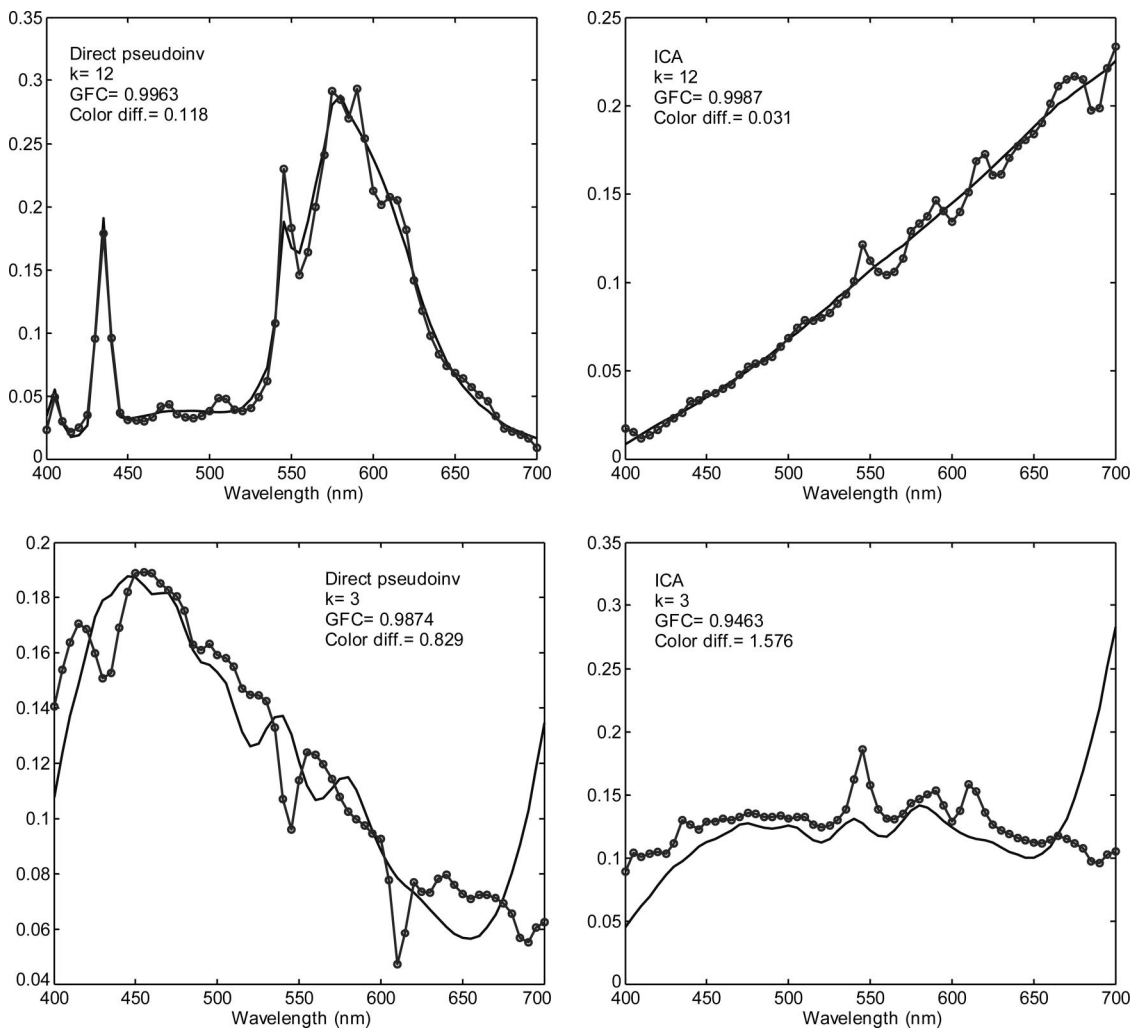

Fig. 5. Examples of SPD recoveries from the computational results and different algorithms, with different numbers, k, of sensors. Original (—) and recovered (o) spectra are shown.

		NMF Euclidean		Direct Pseudoinverse	
		GFC	ΔE^*ab	GFC	ΔE^*ab
$k = 3$	Mean	0.89881	4.39	0.90120	3.03
	SD	0.07802	2.93	0.08220	2.83
$k = 6$	Mean	0.81420	11.92	0.81241	11.90
	SD	0.18021	7.21	0.18462	7.11
$k = 9$	Mean	0.68772	16.72	0.68283	16.54
	SD	0.05310	5.44	0.05311	5.65

metrics should be used because a single quality number may not possibly show significant variations [30].

4. Experimental Results

We next used real data obtained from the same Retiga 1300 digital CCD color camera from QImaging under the same conditions to recover the spectra of illuminants and compare them with a spectroradiometer. The camera outputs were corrected for any nonlinearity by capturing the six gray patches of the GretagMacBeth ColorChecker and simultaneously measuring their radiance with a PR650 spectroradiometer from Photoresearch, Chatsworth, California, USA. We averaged the sensor outputs over a 10×10 pixel image fragment and fixed the camera aperture at 5.6. The dark current was subtracted from the camera sensors, and all the sensor responses were normalized by the corresponding exposure times.

The experimental data to be applied in Eq. (2) were now the camera responses for the achromatic chip number 19 of the GretagMacBeth ColorChecker when illuminated by the following commercial fluorescent lights: Digilite, Trilite, and Opus (Bowens International Limited, Essex, UK) together with a combination of the three lamps. As explained in Sec-

tion 2, the RGB camera outputs were modified using successive cutoff color filters. As a consequence of our computational results we decided to use only the 3-, 6-, and 9-band spectral camera (Fig. 1), as derived from the OG550 and RG630 colored filters.

Table 3 shows the average spectral and colorimetric quality for the experimental results when the NMF Euclidean and the direct pseudoinverse algorithms are used. Recovery quality depended upon the number of sensors, as we have described above for the computational results. The average spectral performance for the direct pseudoinverse method was found to be 0.9 with color differences of around 3 units. Nevertheless, average quality results fell when more than one color filter was used. This clearly differs from the previous computational tests and gives an idea of the influence of noise upon this kind of spectral estimation, with the spiky spectral profile of fluorescents amplifying this effect [5]. Figure 6 shows examples of spectral recoveries using the camera with and without prefilters, in which the plots show once more that good spectral recoveries do not imply good colorimetric performance. These results agree with those found for reflectances in which performance deteriorates concomitantly with an increase in the dimensionality of the linear models, and median ΔE^*ab values within the interval 2.13–3.92 when different dimensional linear models and polynomial methods are used [18].

5. Chromatic Difference Versus Spectral Recovery

The above results suggest that it is possible to convert with considerable accuracy the camera outputs from a neutral surface when illuminated by some kind of fluorescent light to an estimated spectrum for that light. It is impossible to find *a priori* a single correspondence between RGBs and SPDs of illuminants, but can we identify a fluorescent light using the RGB values alone without firstly recovering its spectra? We now show that we can if we take into account that
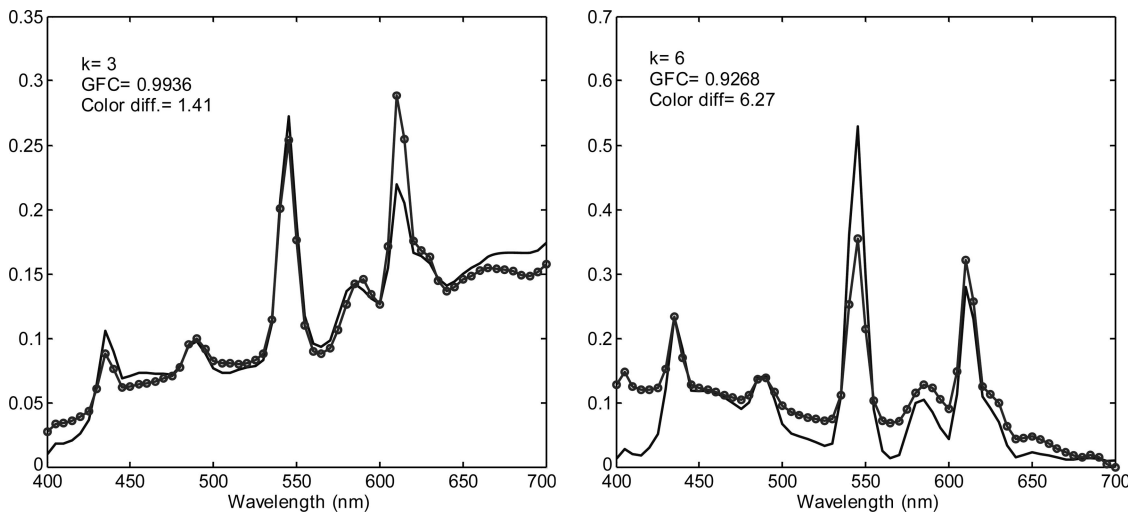

Fig. 6. Examples of experimental SPD recoveries using a real RGB digital camera coupled with different numbers, k, of color filters; the results are for the direct pseudoinverse method. Original (—) and recovered (o) spectra are shown.

Table 4. Average Spectral and Colorimetric Quality Classification of Test Illuminants Using the Direct Pseudoinverse Method with Different Numbers of Sensors[a]

		Simulated Digital Counts		Experimental Results	
		GFC	ΔE^*ab	GFC	ΔE^*ab
$k = 3$	Mean	0.9474	2.33	0.9128	1.67
	SD	0.0811	2.08	0.0637	0.68
$k = 6$	Mean	0.9816	2.20	0.7978	4.33
	SD	0.0153	0.98	0.0492	0.99
$k = 9$	Mean	0.9715	2.36	0.7975	9.26
	SD	0.0312	0.83	0.0052	0.14
$k = 12$	Mean	0.9741	2.37		
	SD	0.0284	0.89		

[a]The results are for computational and experimental results.

the set of commercial available fluorescents is of a reduced size, at least in terms of very different spectral profiles. What we must do first is solve for a set of fluorescents that induces the same sensor outputs when they illuminate a neutral surface. The chip number 19 from the GretagMacBeth ColorChecker will be used as a neutral white surface in the following calculations. In mathematical terms, denoting the sensor outputs of the training illuminants as the $k \times m$ vector, $\mathbf{P}$, (with $m = 82$ SPDs, as used in Section 3), the corresponding solution for the sensor outputs of the test illuminant $\boldsymbol{\rho}$ is also a $k \times m$ vector (with either $m = 20$ SPDs, as in the computational results shown in Section 3, or $m = 6$, as in the Section 4), which is derived by solving for

$$\min\left[\sum_{i=1}^{k}(\rho_i - P_i)^2\right]^{1/2}; \quad (k = 3, 6, 9, 12), \quad (10)$$

where k is the number of sensors (e.g., the RGB camera with successive cutoff filters). This means that we are minimizing the distance between the chromatic coordinates of the test and training illuminants in the sensor output space and not in the spectra domain. With this minimization procedure we tried to solve for the chromaticity region covered by the fluorescents in the chromaticity space (see Fig. 2).

Table 4 shows the average spectral and colorimetric results for the illuminant identification. The training illuminant selected was the closest to the test illuminant in the k-dimensional space of digital counts. On the one hand, our results suggest a good colorimetric quality, with ΔE^*ab values of around 2, although spectral quality is only around 0.97, while on the other hand an increase in the number of colored filters used does not improve recovery quality. This suggests a good performance for a reduced number of sensors with the additional advantage compared with others that no previous classification of fluorescents is needed in the training set of illuminants [17].

6. Summary and Conclusions

We have used four different algorithms based on different mathematical approaches to recover the SPDs of fluorescent lights both computationally and experimentally. The spectral profiles of these lights are characterized by the presence of prominent peaks along the visible spectrum, and these peaks are difficult to recover using PCA with a reduced number of parameters and eigenvectors. First, our computational results suggest that fluorescent lights can be recovered with acceptable spectral and colorimetric accuracy using no information about the spectral sensitivities of the camera sensors or eigenvectors. The greater the number of sensors the better the computational results, whatever the algorithm used, although NMF, ICA, and direct pseudoinverse always surpass the spectral and colorimetric quality of recoveries deriving from PCA. Another difference between the algorithms is that NMF algorithms allow the use of variable ranks of factorization, u, but the ICA [28] does not converge appropriately for $u < 29$ and acceptable results are obtained only for $u \geq 25$.

Apart from the different objective functions used by the NMF algorithms, they differ in terms of computation times. The times of the Euclidean distance algorithm tend to be less than the divergence algorithm but the latter involves fewer floating-point operations [34]. We studied the performance of the Euclidean and the divergence algorithms in comparison with the ICA and the direct-mapping approach. The computational results show slight differences between the Euclidean and divergence algorithms, but it is not clear which outperforms the other in terms of time and computational compression. Although NMF algorithms may reduce the computational cost of spectral devices, our experiments suggest that ICA, and in particular direct pseudoinverse, due to its simplicity, outperforms the NMF approaches, even for fluorescent lights and even using a reduced training set of illuminants. The relatively low quality of the experimental recoveries when compared with our earlier findings may be surprising, particularly the results that suggest a decreasing trend in quality concomitant with an increase in the number of sensors [7]. On the contrary, the use of fluorescents gives an idea of the influence in the direct pseudoinverse method of the spectral gamut produced by the training and test sets of illuminants. The colors produced by the daylight spectra are much reduced when compared to the gamut produced by the fluorescents, and thus it is difficult to find a good correspondence between test RGBs and training spectra for fluorescent lights when the direct pseudoinverse is applied.

We have also shown that it is possible to map test fluorescents within the sensor-output space of the camera by solving for a set of fluorescents that induces the same sensor outputs when illuminating a neutral surface. The results agree with previous algorithms that seek illuminants for color constancy using color by correlation [35] in which case the chromaticity coordinates of an unknown scene illuminant are determined by seeking the correlation between the R, G, and B in an image and a training set of RGBs derived from a large image database reproduced under different illuminant conditions. Our ex-

perimental results go to support previous results indicating the suitability of using a reduced number of sensors and rank of factorization. Although spectral and colorimetric quality are not as good as with simulated digital counts, it is possible to identify fluorescent spectra using a naive RGB digital camera without the constraint of increasing the dimensionality of camera signals by incorporating narrowband filters. This could be an alternative way of identifying spectra using spectral devices with a small number of parameters when it is not possible to have access to a spectroradiometer.

References

1. F. H. Imai, R. Berns, and D.-Y. Tzeng, "A comparative analysis of spectral reflectance estimated in various spaces using a trichromatic camera system," J. Imaging Sci. Technol. **44,** 280–371 (2000).
2. J. Hardeberg, F. Schmitt, and H. Brettel, "Multispectral color image capture using a liquid crystal tunable filter," Opt. Eng. **41,** 2532–2548 (2002).
3. F. H. Imai and R. S. Berns, "Spectral estimation of oil paints using multi-filter trichromatic imaging," in *Proceedings of the Ninth Congress of the International Colour Association* (Rochester, 2001), pp. 504–507.
4. J. Hernández-Andrés, J. L. Nieves, E. Valero, and J. Romero, "Spectral-daylight recovery by use of only a few sensors," J. Opt. Soc. Am. A **21,** 13–23 (2004).
5. M. A. Lopez-Alvarez, J. Romero, R. L. Lee, Jr., and J. Hernández-Andrés, "Designing a practical system for spectral imaging of skylight," Appl. Opt. **44,** 5688–5695 (2005).
6. M. A. López-Álvarez, J. Hernández-Andrés, E. M. Valero, and J. Romero, "Selecting algorithms, sensors, and linear bases for optimum spectral recovery of skylight," J. Opt. Soc. Am. A **24,** 942–956 (2007).
7. J. L. Nieves, E. Valero, S. M. C. Nascimento, J. Hernández-Andrés, and J. Romero, "Multispectral synthesis of daylight using a commercial digital CCD camera," Appl. Opt. **44,** 5696–5703 (2005).
8. C.-C. Chiao, D. Osorio, M. Vorobyev, and T. W. Cronin, "Characterization of natural illuminants in forests and the use of digital video data to reconstruct illuminant spectra," J. Opt. Soc. Am. A **17,** 1713–1721 (2000).
9. S. M. C. Nascimento, F. P. Ferreira, and D. H. Foster, "Statistics of spatial cone-excitation ratios in natural scenes," J. Opt. Soc. Am. A **19,** 1484–1490 (2002).
10. J. Romero, A. García-Beltrán, and J. Hernández-Andrés, "Linear bases for representation of natural and artificial illuminants," J. Opt. Soc. Am. A **14,** 1007–1014 (1997).
11. J. Hernández-Andrés, J. Romero, A. García-Beltrán, and J. L. Nieves, "Testing linear models on spectral daylight measurements," Appl. Opt. **37,** 971–977 (1998).
12. J. Hernández-Andrés, J. Romero, J. L. Nieves, and R. L. Lee, Jr., "Color and spectral analysis of daylight in southern Europe," J. Opt. Soc. Am. A **18,** 1325–1335 (2001).
13. W. K. Pratt and C. E. Mancill, "Spectral estimation techniques for the spectral calibration of a color image scanner," Appl. Opt. **14,** 73–75 (1975).
14. S. Tominaga, S. Ebisui, and B. A. Wandell, "Scene illuminant classification: brighter is better," J. Opt. Soc. Am. A **1,** 55–64 (2001).
15. S. Tominaga, "Natural image database and its use for scene illuminant estimation," J. Electronic Imaging **11,** 434–444 (2002).
16. S. Tominaga and B. A. Wandell, "Natural scene-illuminant estimation using the sensor correlation," in *Proceedings of IEEE 90* (IEEE, 2002), pp. 42–56.
17. S. Tominaga and H. Haraguchi, "A spectral imaging method for classifying fluorescent scene illuminants," in *Proceedings of the Tenth Congress of the International Colour Association* (Granada, 2005), pp. 193–196.
18. V. Cheung, S. Westland, C. Li, J. Hardeberg, and D. Connah, "Characterization of trichromatic color cameras by using a new multispectral imaging technique," J. Opt. Soc. Am. A **7,** 1231–1240 (2005).
19. E. M. Valero, J. L. Nieves, S. M. C. Nascimento, K. Amano, and D. H. Foster, "Recovering spectral data from natural scenes with an RGB digital camera," Color Res. Appl. (to be published).
20. W. Xiong and B. Funt, "Independent component analysis and nonnegative linear model analysis of illuminant and reflectance spectra," in *Proceedings of the Tenth Congress of the International Colour Association* (Granada, 2005), pp. 503–506.
21. S. Bergner and M. S. Drew, "Spatiotemporal-chromatic structure of natural scenes," presented at the International Conference on Image Processing, Genova, Italy, 11–14 Sept. 2005.
22. L. T. Maloney and B. A. Wandell, "Color constancy: a method for recovering surface spectral reflectance," J. Opt. Soc. Am. A **3,** 23–33 (1986).
23. M. D'Zmura and G. Iverson, "Color constancy. I. Basic theory of two-stage linear recovery of spectral descriptions for lights and surfaces," J. Opt. Soc. Am. A **10,** 2148–2165 (1993).
24. K. Barnard, L. Martin, B. Funt, and A. Coath, "A data set for color research," Color Res. Appl. **27,** 147–151 (2002).
25. Commission Internationale d'l'Eclairage, Colorimetry, Publication CIE No. 15.2 (1986).
26. P. Paatero and U. Tapper, "Positive matrix factorization: a non-negative factor model with optimal utilization of error estimates of data values," Environmetrics **5,** 111–126 (1994).
27. A. J. Bell and T. J. Sejnowski, "An information-maximization approach to blind separation and blind deconvolution," Neural Comput. **7,** 1129–1159 (1995).
28. D. D. Lee and H. S. Seung, "Algorithms for non-negative matrix factorization," Adv. Neural Info. Proc. Syst. **13,** 556–562 (2001).
29. A. Hyvärinen, "Fast and robust fixed-point algorithms for independent component analysis," IEEE Trans. Neural Netw. **10,** 626–634 (1999).
30. F. H. Imai, M. R. Rosen, and R. S. Berns, "Comparative study of metrics for spectral match quality," in *Proceedings of the First European Conference on Colour in Graphics, Imaging and Vision* (Society for Imaging Science and Technology, 2002), pp. 492–496.
31. M. J. Vrhel, R. Gershon, and L. S. Iwan, "Measurement and analysis of object reflectance spectra," Color Res. Appl. **19,** 4–9 (1994).
32. G. Finlayson, "Spectral sharpening: what is it and why is it important," in *Proceedings of the First European Conference on Colour in Graphics, Imaging and Vision* (Society for Imaging Science and Technology, 2002), pp. 230–235.
33. National Institute of Standards and Technology (NIST) http://physics.nist.gov/Divisions/Div844/Newrad/abstracts/NadalPoster.htm.
34. S. Wild, "Seeding non-negative matrix factorizations with the spherical K-Means clustering," M.Sc. thesis (University of Colorado, 2003).
35. G. D. Finlayson, S. D. Hordley, and P. M. Hubel, "Color by correlation: a simple, unifying framework for color constancy," IEEE Trans. Pattern Anal. Mach. Intell. **23,** 1209–1221 (2001).